Article

Optimal Dual Active Bridge DC-DC Converter Operation with Minimal Reactive Power for Battery Electric Vehicles Using Model Predictive Control

Nasr Guennouni [1,*], Ahmed Chebak [1] and Nadia Machkour [1,2]

1   Green Technology Institute, Mohammed VI Polytechnic University, 43150 Benguerir, Morocco; ahmed.chebak@um6p.ma (A.C.); nadia.machkour@um6p.ma (N.M.)
2   Structural Engineering, Intelligent Systems and Electrical Energy Laboratory, Ecole Nationale Supérieure des Arts et Métiers, Hassan II University of Casablanca, 20670 Casablanca, Morocco
*   Correspondence: nasr.guennouni@um6p.ma; Tel.: +212-699895981

Abstract: The dual active bridge DC-DC converter is a promising power converter used in several applications. Much research has been focusing on the study of such a converter from different angles. In this paper, an optimal design of the DAB converter is proposed to provide minimal reactive power in addition to reduced weight and size for the converter magnetic components in order to assure the DC-DC conversion stage of battery electric vehicles' powertrains. Two modes of operation are considered in order to fulfill such a requirement and minimize reactive power of the converter (circulating current/conduction losses): an optimal extended phase shift (EPS) modulation along with an optimal triangular phase shift (TrgPS) modulation. The operation of the DAB converter under the two modes is being driven using a model predictive controller. Simulation results using MATLAB/Simulink presented in the paper show that the operation of the DAB converter for such an application is optimal when operating under optimal TrgPS modulation. In addition to the aforementioned features, it also solves many other concerns, such as transient load fluctuation and input voltage disturbance effects, and provides ease of control.

Keywords: dual active bridge DC-DC converter; battery electric vehicles; model predictive control

1. Introduction

EVs can be classified into three major categories [1]. As a first step towards fully electric vehicles, hybrid electric vehicles (HEV) have the feature of gathering two different power sources since their powertrains operate by combining both an internal combustion engine (ICE) and an electric propulsion system in order to reduce fuel consumption and improve the vehicle's range and performance [2]. Even if this technology of EVs represents the most important portion in the market and is considered the most mature EV technology for now, HEVs are not spared from fuel and oil consumption and consequently it is not considered as a 100% environmentally friendly technology. On the other hand, fuel cell electric vehicles (FCEV) are fully electric vehicles and are powered by a fuel cell which can be combined with an auxiliary battery or a supercapacitor [3]. However, this type of EV has many limitations and drawbacks for now; since the share of the market of fuel cells is still tiny, it is still not a mature technology yet, which makes FCEVs suffer from high prices and many distribution issues [3]. Another type of EVs consists of battery electric vehicles (BEV) where the powertrain is simply powered by a traction battery as a main energy source. In comparison with the aforementioned technologies, this type of EV is considered to be the most suitable to address environmental issues and the energy crisis since they are the most affordable vehicles providing zero gas emissions [4]. That said, the following analysis will focus on BEVs.

Researchers are focusing on three major fields to improve the powertrains of BEVs: electric motors, energy storage, and power electronics. In an electric powertrain, the

power flow between the energy storage system (ESS) and the traction motor needs to be conditioned and managed through the use of a power converter [5]. This energy conditioning is achieved using a two-stage power converter. First, a step-up DC-DC power converter is used in order to match the battery voltage to the DC bus voltage. Then, the DC bus voltage is used to feed the DC-AC power converter (inverter) to drive the electric motor which is usually an AC machine. An optimal design of such a power converter helps in achieving a longer lifecycle of the ESS, a better motor performance, an optimal use of ESS and traction motor, and, last but not least, a better overall powertrain efficiency. Many researchers have employed model-based system engineering (MBSE) in order to design electric vehicles [6–9]. In [10], the authors presented a general scheme for the operational view of the power converter dedicated to electric traction with onboard ESS. According to the work realized, the dual active bridge (DAB) converter is a suitable architecture to fulfill the requirements of the DC-DC stage conversion of a power converter for electric traction with onboard ESS. In fact, the DAB provides bidirectional power flow, galvanic isolation (guarantees the user safety), and high efficiency in addition to a controllable boosting ratio to match the high DC bus voltage from a much lower voltage source (the traction battery, in our case). Consequently, the aim of this paper is to analyze the operation of such a converter and its ability and performance to fulfill the DC-DC stage conversion requirements of a power converter dedicated to the powertrain of BEVs. The paper is organized as follows: First, the DAB DC-DC converter is presented in Section 2 along with its possible operation modes. Section 3 focuses on the control of such a converter by selecting arbitrarily a model predictive controller and presents different steps to design such a controller to drive the DAB DC-DC converter and analyzes its characteristics. Finally, Section 4 proposes an optimal operation, design, and control of the DAB DC-DC converter that satisfy the requirements of weight, compacity, efficiency, and ease of control which makes the power converter more suitable for BEVs' powertrains.

2. Dual Active Bridge DC-DC Converter

2.1. Global Context

The dual-active-bridge is characterized by a symmetrical architecture. It consists of active power switches that guarantee a bidirectional power flow depending on its control [11,12]. The topology of a DAB converter is shown in Figure 1, along with its simplified equivalent circuit in Figure 2, assuming the ideal power switches and transformer. The power converter has the ultimate advantage to provide galvanic isolation. As shown in Figure 1, a DAB converter consists of a transformer, connected to two H-bridges in its primary and secondary. A conventional and traditional way to control the converter consists of switching semiconductor devices with 50% duty cycles which results in generating two square voltages v_{ab} and v_{cd}.

The transformer leakage inductance (or an additional inductor) serves as the instantaneous energy storage element. Since the converter is bidirectional, and depending on the power flow direction desired, the two bridges can be considered as primary or secondary. A DAB is ideal for energy storage systems (ESSs) and power electronic transformers (PETs) due to its numerous advantageous characteristics such as wide voltage conversion gain range. Moreover, DAB DC-DC converter is ideal for interfacing ESSs such as batteries or super-capacitors, where voltage varies drastically depending on their state of charge. DAB DC-DC converter also provides ZVS-on property (if a suitable control is applied) and the ability to reach high efficiency. However, even if the DAB DC-DC converter provides many interesting features as mentioned earlier, the converter can be subject to the reactive power issue (circulating current). As mentioned before, a DAB is conventionally modulated using a single phase shift (SPS) (50% duty ratio for power switches) and the reactive power becomes more important and causes efficiency decrease drastically when the voltage gain is far from unity. Similar to the one in power systems, the reactive power does not transfer any energy, but produces power device conduction losses and transformer copper losses. The reactive power when it comes to the DAB DC-DC converter will always be an issue

as long as the square voltages generated by the H-bridges and the inductor current are not in phase, and its amount increases as the voltage gain moves away from unity. This phenomenon can be explained using the phasor diagram in Figure 3.
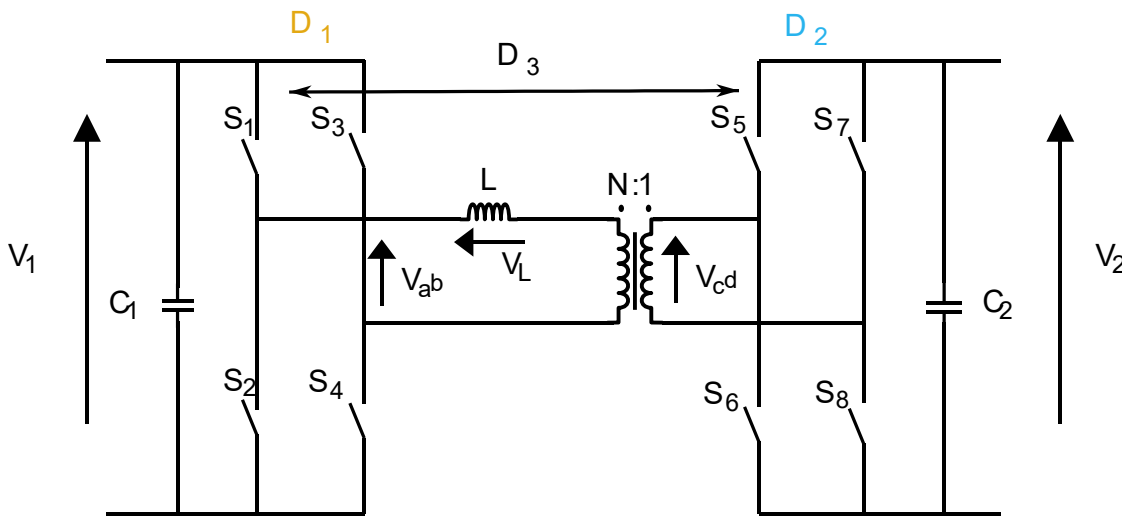

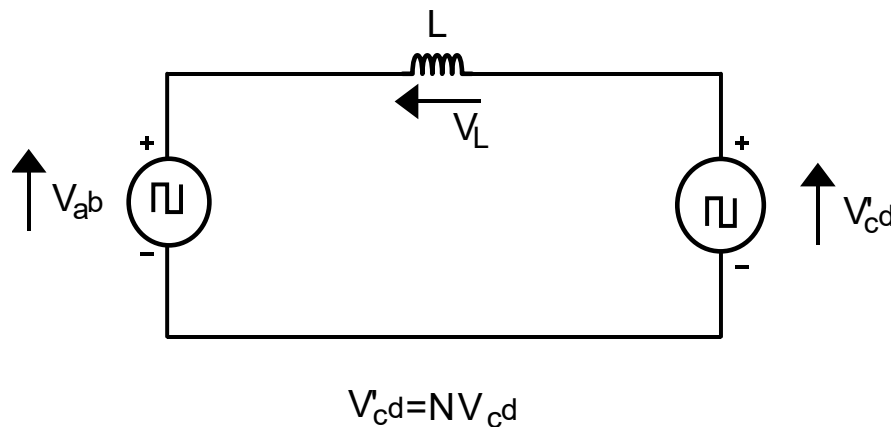**Figure 1.** Dual active bridge DC-DC converter topology.

$$V'_{cd} = N V_{cd}$$

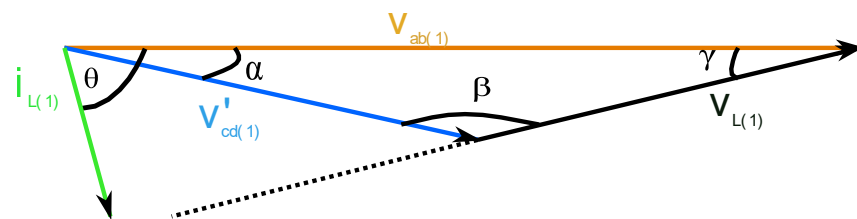**Figure 2.** Simplified equivalent circuit of DAB DC-DC converter.

Figure 3. Phasor diagram representing fundamental components of voltages and current.

The angles in the phasor diagram will systematically obey the law of sines:

$$\begin{cases} \beta + \gamma = \pi - \alpha \\ \frac{\sin \gamma}{\sin \beta} = \frac{\left| \vec{v_{cd1}} \right|}{\left| \vec{v_{ab1}} \right|} = d \\ \theta = \frac{\pi}{2} - \gamma \end{cases} \tag{1}$$

and since α is the angle between $v_{ab(1)}$ and $v'_{cd(1)}$, this implies that α is directly related to the phase shift ratio between the two H-bridges (primary and secondary), as $\alpha = D_3 \pi$.

Consequently, a small voltage gain $d = NV_2/V_1$ would imply a small γ and a large θ according to (1) and Figure 3 where $d < 1$. An increase in θ (the angle between $v_{ab(1)}$ and $i_{L(1)}$) will inherently increase the reactive power in the circuit. In order to eliminate (or at least minimize) the reactive power, an instinctive approach comes to mind. If one adjusts the $v_{ab(1)}$ and $v'_{cd(1)}$ duty ratios so their amplitudes could be equal, in that case, the resulting $v_{L(1)}$ would lead to a smaller θ compared to Figure 3 and the reactive power would be minimized. It is obvious that the phase shift ratios can be adjusted more properly to reduce the reactive power, and the proper selection of D_1, D_2, and D_3 to minimize the reactive power is still an active DAB research topic [13–15]. Depending on which duty ratios to adjust, the DAB modulation methods can be classified as:

- Single phase shift (SPS), $D_1 = D_2 = 1$, where in order to regulate and control output voltage, only D_3 is controlled.
- Dual phase shift (DPS), a modulation technique which offers an additional degree of freedom besides D_3, to eliminate/minimize the circulating current, where only D_1 or D_2 is controlled (also known as extended phase shift (EPS)) [16], or where both D_1 and D_2 are controlled, but keeping $D_1 = D_2$ [17–19].
- Triple phase shift (TPS), where D_1, D_2, and D_3 are controlled independently [13,15,20–22].

Even though EPS and DPS are able to minimize the DAB circulating current to some limit, their phase shift ratios can only be locally optimized. On the other hand, with different operating modes and three degrees of freedom, it gets more complicated (compared to SPS and DPS) to find the global optimal duty ratios for the converter. A first approach consists of approximating square voltages and inductor currents based on fundamental components [20,21]. The optimal duty ratios are obtained by using several methods such as: maximizing fundamental power factor [23], minimizing amplitudes of i_L [20], or minimizing fundamental reactive power [21]. The derivation steps of these techniques are straightforward; however, the fundamental component approximation of the square voltages introduces error, especially when either D_1 or D_2 is close to 0. That said, various operating modes of the DAB DC-DC converter have to be taken into account in order to find global optimal duty ratios in TPS, since the expressions of the current and power are not the same for each mode. In [11], the authors reduced DAB operation (buck/forward) into five different modes and achieved optimal duty ratios; however, the derivation process was incomplete and unsatisfactory. Therefore, based on the work presented in [11], the authors in [13] meticulously achieved global optimal duty ratios using the Karush–Kuhn–Tucker (KKT) method. Authors in [14] used the Lagrange multiplier method (LMM) which led them to optimal duty ratios; however, some of the operating modes were not taken into account. The authors in [15] emphasized that the LMM used in [13,14] (the KKT method is considered as an LMM method) encounters a concern about adequacy as a consequence of the non-convex feasibility of regions in some of the operating modes. The optimal duty ratios in [15] were deduced using minimal root mean square (RMS) values of the inductor current i_L and results of the optimal duty ratios were similar to the ones achieved by [13,14]. The authors in [13–15] reached global optimal duty ratios; however, the methods used to reach such results are not that practical since a considerable optimization for each mode is required. Hence, in the upcoming analysis, we will use the analysis proposed by [22] since it takes into account the problems and difficulties encountered in previous proposed analyses and suggests global optimal duty ratios for various operating modes of the DAB DC-DC converter, as it can be shown in upcoming sections and subsections.

2.2. Optimal Operation Modes

A DAB DC-DC converter is a bidirectional power converter; that said, the converter allows a forward power flow or backward power flow. In addition, a DAB DC-DC converter can operate as a buck or boost converter depending on its voltage gain d. Consequently, there are four different scenarios a DAB can operate based on its power flow P along with its voltage gain d. Only two scenarios (forward/buck and backward/boost) among the four possible cases are of interest when it comes to BEVs in order to assure the DC-DC conversion

stage. It is possible to transform the aforementioned scenarios to the forward/buck scenario to simplify the analysis [22]. D_f is the phase shift between the fundamental components of v_{ab} and v_{cd} [13,23] and can be expressed as (2) and according to [13], and the output power can be expressed using Fourier series as (3):

$$D_f = \frac{D_2}{2} - \frac{D_1}{2} + D_3 \tag{2}$$

$$P = \sum_{k=1,\,3,\,5\ldots} \frac{4NV_1V_2T_s \sin\alpha \sin\beta \sin\gamma}{(k\pi)^3 L} \tag{3}$$

where $\alpha = kD_1\pi/2$, $\beta = kD_2\pi/2$, and $\gamma = kD_f\pi$. According to (4), D_f must be in range of $[-1/2; 1/2]$ to guarantee monotonicity between P and D_f. For the forward/buck scenario ($P > 0$; $d < 1$), the constraints of D_1, D_2, and D_f are: $D_1, D_2 \in (0, 1]$, and $D_f \in (0; 1/2]$. Based on these constraints and taking v_{ab} as a reference [22], one can obtain five possible operating modes, as shown in Figure 4.
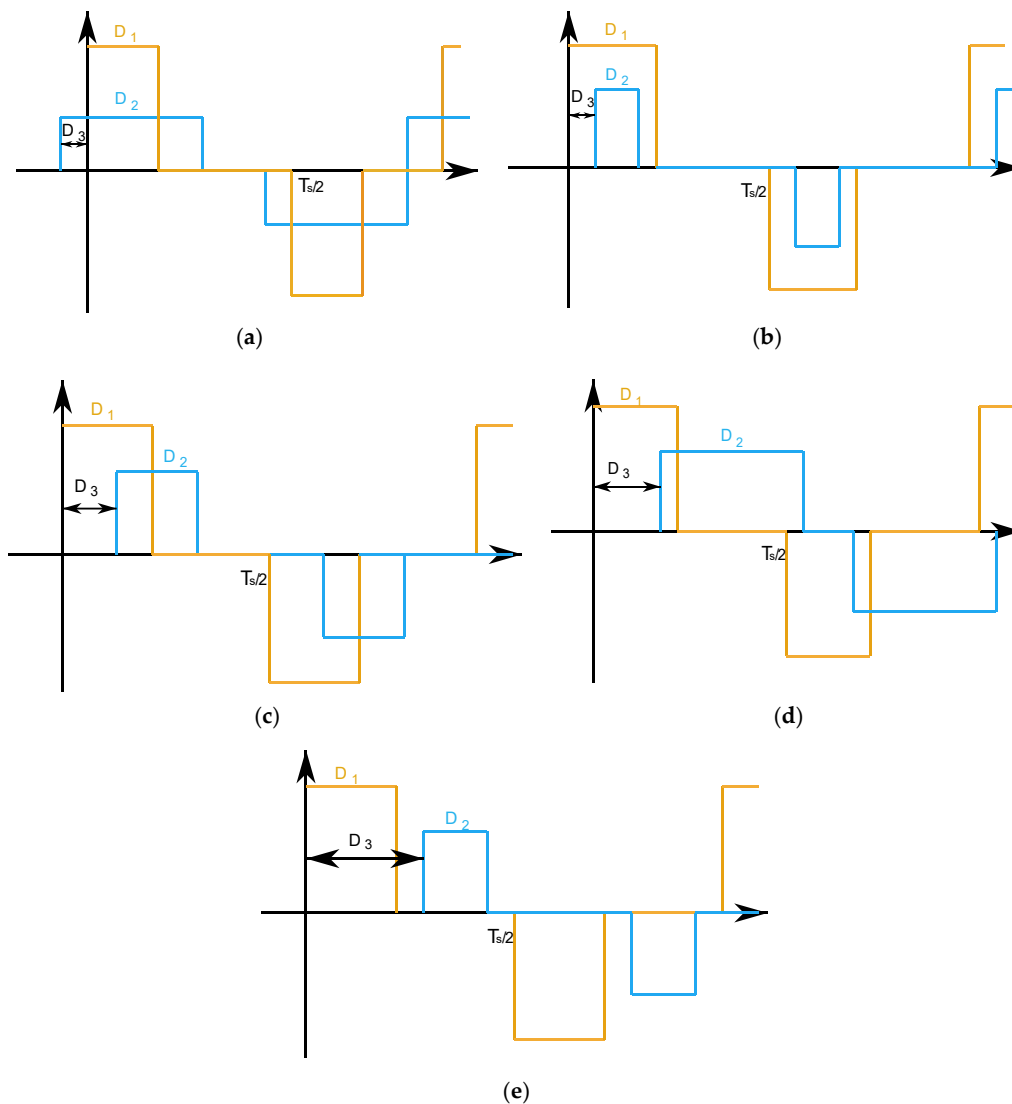
Figure 4. Different operations modes of DAB DC-DC converter in forward/buck case scenario: (**a**) mode 1: $D_3 \leq 0$; (**b**) mode 2: $0 \leq D_3 \leq D_1$, $D_2 + D_3 \leq D_1$; (**c**) mode 3: $0 \leq D_3 \leq D_1$, $D_2 + D_3 \geq D_1$; (**d**) mode 4: $0 \leq D_3 \leq D_1$, $D_2 + D_3 \geq 1$; (**e**) mode 5: $D_3 \geq 1$.

Taking v_{ab} as a reference, these operating modes consist of:

- Mode 1, Figure 4a: the rising edge of v'_{cd} leads that of v_{ab}, where $D_3 \leq 0$. Based on the constraint $D_f > 0$, $D_2/2 + D_3 > D_1/2$ is derived according to (2), and the constraint leads to having the falling edge of v'_{cd} lag that of v_{ab}.
- Modes 2–4, Figure 4b–d: the rising edge of v'_{cd} is located between the rising and falling edges of v_{ab}, where $0 \leq D_3 \leq D_1$. However, the difference between the three modes appears in the falling edge of v'_{cd} which is decided by $D_2/2 + D_3$.
- Mode 5, Figure 4e: the rising edge of v'_{cd} lags the falling edge of v_{ab}, where $D_3 \geq D_1$. Based on the constraint $D_f \leq 1/2$, $D_2/2 + D_3 \leq 1$ is derived according to (2), which means the falling edge of v'_{cd} is within the same half-cycle as its rising edge.

According to [22], for the same power rate, modes 1, 2, and 5 can be brought to mode 3 delivering the same power with less RMS current and therefore less power losses. Consequently, only the analysis of modes 3 and 4 is considered in the following sections, and normalized power and current stress are derived for the two modes by taking into consideration the following definition [22]:

$$\begin{cases} I_n = \frac{I_s}{I_b}, \ I_b = \frac{V_1}{4fL} \\ P_n = \frac{P}{P_b}, P_b = \frac{dV_1^2}{2fL} \end{cases} \tag{4}$$

where:

I_b, P_b: base current stress and power
I_n, P_n: normalized current stress and power
I_s, P: rated current stress and power
$d = NV_1/V_2$: voltage gain
$f = 1/T_s$: switching frequency and period
V_1: input voltage
V_2: output voltage

The expressions of normalized current stress and power for modes 3 and 4, respectively, are presented in (5) and (6):

$$\begin{cases} I_{n3} = (1-2d)D_1 + dD_2 + 2dD_3 \\ P_{n3} = \frac{(D_1D_2 + 2D_1D_3 - D_1^2 - D_3^2)}{2} \end{cases} \tag{5}$$

$$\begin{cases} I_{n4} = (1-d)D_1 + 2D_f \\ P_{n4} = \frac{4D_f - 4D_f^2 - (1-D_1)^2 - (1-D_2)^2}{4} \end{cases} \tag{6}$$

Following the constraints on each D_1, D_2, D_3, and D_f and by studying the conditions where I_n is minimal, Table 1 summarizes the optimal duty ratios for the forward/buck and backward/boost cases depending on the power requested from the load.

Table 1. Optimal duty ratios for the DAB converter in both forward/buck and backward/boost scenarios [22].

Voltage Gain	Power	Duty Ratios
$d < 1$	$P_n \epsilon \left[0, \frac{d(1-d)}{2} \right]$ $P_n \epsilon \left[\frac{d(1-d)}{2}, \frac{1}{4} \right]$	$\begin{cases} D_1 = \sqrt{\frac{2dP_n}{1-d}} \\ D_2 = \frac{D_1}{d}, D_3 = 0 \end{cases}$ $\begin{cases} D_1 = 1 - (1-d)\sqrt{\frac{1-4P_n}{1-2d+2d^2}} \\ D_2 = 1, D_3 = \frac{D_1-d}{2(1-d)} \end{cases}$
$d > 1$	$P_n \epsilon \left[-\frac{d-1}{2d^2}, 0 \right]$ $P_n \epsilon \left[-\frac{1}{4}, -\frac{d-1}{2d^2} \right]$	$\begin{cases} D_2 = \sqrt{-\frac{2P_n}{d-1}} \\ D_1 = \frac{D_2}{d}, D_3 = 0 \end{cases}$ $\begin{cases} D_2 = 1 - (d-1)\sqrt{\frac{1+4P_n}{2-2d+d^2}} \\ D_1 = 1, D_3 = \frac{1-dD_2}{2(d-1)} \end{cases}$

3. Model Predictive Control (MPC) for Minimum Global Reactive Power of DAB DC-DC Converter

3.1. General Control Scheme for Minimum Global Reactive Power of DAB DC-DC Converter

This section presents a DAB general control scheme to regulate the output voltage with minimum reactive power. D_f is chosen to regulate the output voltage since D_f will in any case always be monotonically related to the output power, and according to (2), $D_f \epsilon [-1/2; 1/2]$, so such a parameter is useful in order to make a distinction between operating scenarios in steady state ($P < 0$; $P > 0$; $d < 1$; $d > 1$) and thus convenient for control implementation. This is not the case for D_1 and D_2 or D_3, since D_1 and $D_2 \epsilon [0; 1]$, and D_3 is always 0 in mode 3. Figure 5 shows the general control scheme for the converter. The secondary-side DC bus voltage V_2 is compared with its reference V^*_2 to generate the voltage error, and through a controller, D_f is obtained. D_f is limited in the range $[-0.5; 0.5]$ to ensure a monotonic relationship between D_f and output power. V_1 and V_2 are used to calculate the voltage gain. D_f and d together decide D_1 and D_2 according to Table 2. Slow loops should be used to generate the actual D_1 and D_2 to avoid the influence of the mode's selection on dynamic response (in case of operation of the DAB using EPS at full load). D_3 is calculated based on (3). Finally, gate signals are generated from D_1, D_2, and D_3.
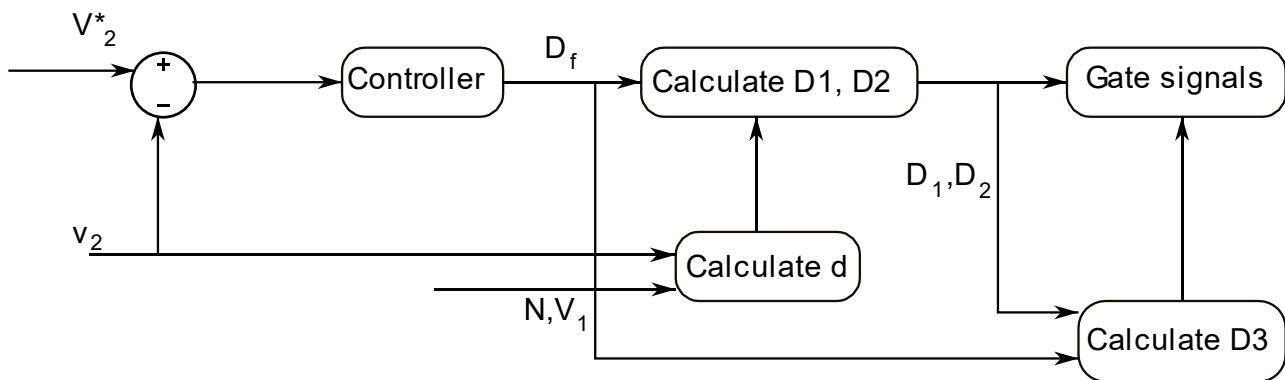
Figure 5. General control scheme to achieve minimum reactive power.

Table 2. Global optimal duty ratios expressions using the control variable D_f [22].

Voltage Gain	Duty Ratio between Fundamentals D_f	Duty Ratios
$d < 1$	$D_f \epsilon \left[0, \frac{1-d}{2}\right]$ $D_f \epsilon \left[\frac{1-d}{2}, \frac{1}{2}\right]$	$\begin{cases} D_1 = \frac{2dD_f}{1-d} \\ D_2 = \frac{2D_f}{1-d} \\ D_3 = 0 \end{cases}$ $\begin{cases} D_1 = 1 - \frac{(1-d)(1-2D_f)}{d} \\ D_2 = 1 \\ D_3 = D_f - \frac{D_2}{2} + \frac{D_1}{2} \end{cases}$
$d > 1$	$D_f \epsilon \left[-\frac{d-1}{2d}, 0\right]$ $D_f \epsilon \left[-\frac{1}{2}, -\frac{d-1}{2d}\right]$	$\begin{cases} D_1 = -\frac{2dD_f}{d-1} \\ D_2 = -\frac{2D_f}{d-1} \\ D_3 = 0 \end{cases}$ $\begin{cases} D_1 = 1 \\ D_2 = 2 - d + 2(1 - dD_f) \\ D_3 = D_f - \frac{D_2}{2} + \frac{D_1}{2} \end{cases}$

For the upcoming analysis, the input voltage source is considered as constant. Therefore, the focus is on the dynamics of the output filter C and the load R_L, and the DAB DC-DC converter can be considered as a variable power source once its average model is derived [24–26]:

$$C\frac{dv_2(t)}{dt} = \frac{P}{V_2} - \frac{v_2(t)}{R_L} \tag{7}$$

where $v_2(t)$ is the variable representation of the output voltage V_2 in a steady-state condition. Only the forward/buck case analysis is presented since the analysis of the backward/boost case can be realized similarly due to the symmetrical feature presented in Tables 1 and 2.

3.2. Design of Model Predictive Controller

Model predictive control has earned a reputation as a reliable and robust control strategy during last decade. It simply uses the system model in order to predict its output response in the future. Such a control strategy provides the ability to select an optimal control action that minimizes a chosen cost function. When it comes to power electronics, MPC represents a reliable substitute of traditional control schemes based on PID control. In fact, MPC shows a better dynamic performance and provides the possibility of integrating multiple inputs/outputs along with their constraints, respectively; in addition, it also makes it possible to take into account the models' and constraints' nonlinearities. In some fields, the extraction of an accurate system model may be not that easy and thus represents a weakness of MPC; however, this drawback is eliminated when it comes to the power electronics field, since accurate and reliable models are available and are not hard to be established [27,28]. MPC generally consists of three steps: the system prediction model, seeking optimal value, and feedback correction. The derivative term of the output voltage represents the varying trend of the output voltage. To obtain the predictive value of the output voltage in the next control interval, the derivative term of the output voltage should be discretized.

$$\frac{dv_2}{dt} = \frac{v_2(k+1) - v_2(k)}{t_{k+1} - t_k} = \frac{v_2(k+1) - v_2(k)}{T_h} \tag{8}$$

For operation in optimal triangular phase shift (TrgPS) modulation (optimal operation within mode 3), the predicted expression of the output voltage for DAB DC-DC converters can be shown as (10) where uo(k) and uo($k + 1$) represent the output voltages at the kth and ($k + 1$)th sampling instant. The prediction expression of the output voltage is relative to the load resistance. When the load is changed, the prediction value will be not accurate. Therefore, the load current i_2 is introduced into the prediction model to replace the load resistance, and the final prediction expression is expressed as (10).

$$v_2(k+1) = -\frac{2D_f^2 dNV_1}{2f^2 LC(d-1)} - \frac{v_2(k)}{RfC} + v_2(k) \tag{9}$$

$$v_2(k+1) = -\frac{2D_f^2 dNV_1}{2f^2 LC(d-1)} - \frac{i_2(k)}{fC} + v_2(k) \tag{10}$$

The aim of the MPC strategy is to track the output voltage with its desired value V_2 rapidly and accurately under all operating conditions. The cost function can be used to evaluate the system state with single or multiple control targets. According to the prediction model and control theory, a simple cost function can be defined as:

$$F(k) = (v_2(k+1) - V_2(k))^2 \tag{11}$$

$$F(k) = \left(-\frac{2D_f^2 dNV_1}{2f^2 LC(d-1)} - \frac{i_2(k)}{fC} + v_2(k) - V_2(k)\right)^2, \tag{12}$$

where the smaller the value of cost function is, the closer the output voltage at the ($k + 1$)th sampling instant is to the desired value at the kth sampling instant after the selected optimized variable is applied in the kth sampling interval. Therefore, the phase shift ratio D_f that minimizes the cost function can be obtained from cost function derivation with respect to D_f and shown as:

$$\begin{cases} D_{fopt} = \frac{\sqrt{1+a}}{b} \\ a = -dNV_1Lf(CdfV_2(k) - Cdfv_2(k) - CfV_2(k) + Cfv_2(k) + di_2(k) - i_2(k)) - 1 \\ b = dNV_1 \end{cases} \quad (13)$$

To reflect the influence of output voltage disturbance on the fundamentals' optimization calculation due to output voltage disturbance, $D_{f,opt}$ is expanded using Taylor's formula at a steady-state point, and the high-order term (more than two orders) is ignored:

$$\begin{cases} D_{fopt} = D_f^* + \frac{1}{2b\sqrt{1+a^*}}(a - a^*) - \frac{1}{4b\sqrt{1+a^*}^3}(a - a^*)^2 \\ D_f^* = \frac{\sqrt{-dNV_1I_2(-1+d)fL}}{dNV_1} \\ a^* = -dNV_1I_2(-1+d)fL - 1 \end{cases} \quad (14)$$

where D_f^* and a^* are steady-state values, which can be estimated from (13), and I_2 is the steady-state load current. Thus, the disturbance produced by the optimization calculation of the PS ratio due to output voltage disturbance can be obtained by

$$\hat{d}_f = \left(\frac{1}{2b\sqrt{1+a^*}} + \frac{a^*}{2b\sqrt{1+a^*}^3} \right)\hat{a} \quad (15)$$

and substituting $\hat{a}$ from (14) and (15) one will get:

$$\hat{d}_f = K_1(K_2(K_3\widehat{v_{2,err}}(k) + \widehat{i_{2,err}}(k)) \quad (16)$$

where $\begin{cases} K_1 = \left(\frac{1}{2b\sqrt{1+a^*}} + \frac{a^*}{2b\sqrt{1+a^*}^3} \right) \\ K_2 = -dnV_1Lf(-1+d) \\ K_3 = -Cf \end{cases}$.

For operation in optimal extended phase shift modulation (optimal operation within mode 4), the predicted expression of the output voltage for DAB DC-DC converters can be shown as (17) and (18).

$$v_2(k+1) = -\frac{0.25\left(8D_f^2d^2 - 8D_f^2d - 8D_fd^2 + 4D_f^2 + 8D_fd + d^2 - 4D_f - 2d + 1\right)}{d^2}\frac{NV_1V_2}{2f^2LC} - \frac{v_2(k)}{R_LfC} + v_2(k) \quad (17)$$

$$v_2(k+1) = -\frac{0.25\left(8D_f^2d^2 - 8D_f^2d - 8D_fd^2 + 4D_f^2 + 8D_fd + d^2 - 4D_f - 2d + 1\right)}{d^2}\frac{NV_1V_2}{2f^2LC} - \frac{i_2(k)}{fC} + v_2(k) \quad (18)$$

The cost function in this case will be expressed as

$$F(k) = \left(-\frac{0.25\left(8D_f^2d^2 - 8D_f^2d - 8D_fd^2 + 4D_f^2 + 8D_fd + d^2 - 4D_f - 2d + 1\right)}{d^2}\frac{NV_1V_2}{2f^2LC} - \frac{i_2(k)}{fC} + v_2(k) - V_2(k) \right)^2 \quad (19)$$

and the expression of $D_{f,opt}$ becomes

$$\begin{cases} D_{fopt} = c\left(b + \sqrt{1+a}\right) \\ c = -\frac{1}{2NV_1(2d^2 - 2d + 1)} \\ b = -2NV_1d^2 + 2NV_1d - NV_1 \end{cases} \quad (20)$$

with

$$a = -16CLNV_1d^4f^2V_2(k) + 16CLNV_1d^4f^2v_2(k) + 16CLNV_1d^3f^2V_2(k) - 16CLNV_1d^4f^2v_2(k)$$
$$- 8CLNV_1d^2f^2V_2(k) + 8CLNV_1d^2f^2v_2(k) - 16LNV_1d^4fi_2(k) + 16LNV_1d^3fi_2(k)$$
$$+ 2(NV_1)^2d^4 - 8LNV_1d^2fi_2(k) - 2(NV_1)^2d^3 + (NV_1)^2d^2 - 1 \tag{21}$$

Extending the expression of $D_{f,opt}$ using Taylor's formula, we get

$$D_{fopt} = D_f^* + \frac{c}{2\sqrt{1+a^*}}(a - a^*) - \frac{c}{4\sqrt{1+a^*}^3}(a - a^*) \tag{22}$$

with

$$D_f^* = \left(b + \sqrt{-16LNV_1d^4fI_2 + 2(NV_1)^2d^4 + 16LNV_1d^3fI_2 - 2(NV_1)^2d^3 - 8LNV_1d^2fI_2 + (NV_1)^2d^2}\right)c \tag{23}$$

$$a^* = -16LNV_1d^4fI_2 + 2(NV_1)^2d^4 + 16LNV_1d^3fI_2 - 2(NV_1)^2d^3 - 8LNV_1d^2fI_2 + (NV_1)^2d^2 - 1 \tag{24}$$

Thus, the disturbance produced by the optimization calculation of the PS ratio due to output voltage disturbance can be obtained by

$$\hat{d}_f = \left(\frac{c}{2\sqrt{1+a^*}} + \frac{ca^*}{2\sqrt{1+a^*}^3}\right)\hat{a} \tag{25}$$

and one can obtain (28) from (23) and (26):

$$\hat{d}_f = K_1(K_2(K_3\hat{v_{2,err}}(k) + \hat{i_{2,err}}(k)) \tag{26}$$

where
$$\begin{cases} K_1 = \left(\frac{c}{2\sqrt{1+a^*}} + \frac{ca^*}{2\sqrt{1+a^*}^3}\right) \\ K_2 = 8d^2NV_1Lf(2d^2 - 2d + 1) \\ K_3 = -Cf \end{cases}.$$

In order to elaborate a model taking into account the conduction losses of the converter, the expression of the power seen by the load is shown in Equation (27), where r_{sc} represents the internal resistance of the switch (the transformer internal resistance is neglected in comparison with the internal resistance of the power switches), and similarly the disturbances of the control variable can be derived following the same previous steps:

$$\begin{cases} P = P_nP_b - rI_1^2 \\ r = 2r_{sc}(1 + N^2) \end{cases} \tag{27}$$

In both case scenarios, a general scheme of the MPC controller is represented in Figure 6 where $\hat{i}_{error}$ is the error between the theoretical and measured currents.
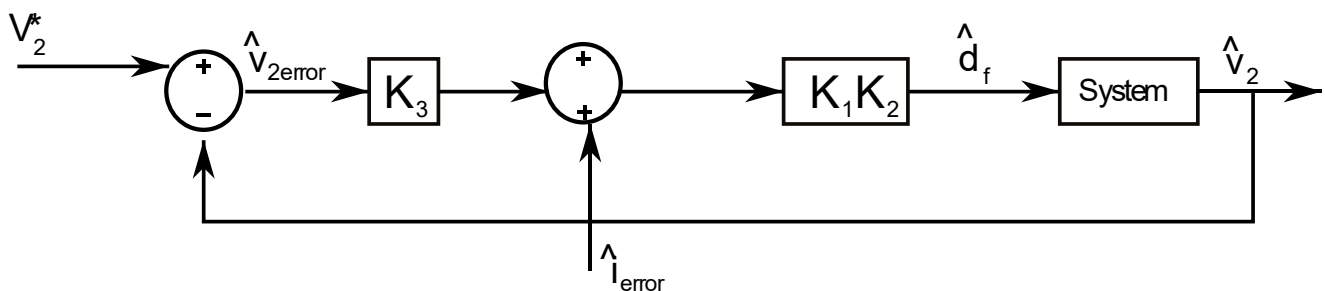

Figure 6. MPC control scheme.

3.3. Analysis of DAB Converter Operation under Optimal Triangular and Optimal Extended Phase Shift Modulations Using MPC

3.3.1. Optimal TrgPS Modulation

The upcoming analysis is realized for a DAB DC-DC converter supposed to deliver a maximum power of 80 kW ($P_n \rightarrow \overline{\frac{d(1-d)}{2}}$ referring to Table 1), and L = 1.57 μH, with V_1 = 288 V, V_2 = 700 V with f = 20 kHz, and C = 100 μF.

As it can be seen in Figure 7 where the nominal power is P = 80 kW, the MPC shows a fast response in order to reach the steady-state desired output value of the output voltage without showing any overshoot and with a negligible relative error. Now when it comes to load variation, Figure 8 shows that the output voltage stays stable even if the load is varying from 80 kW to 48 kW. On the other hand, Figure 9 shows that there is a slight difference when we use the perfect or the conduction loss model since the maximum relative error is estimated by almost 0.5% and 1.4%, respectively, which obviously makes the loss model a more accurate model of the converter. When it comes to the power dissipated in power switches, referring to Figure 9b, it only represents approximately 0.25%. That said, the efficiency of the DAB DC-DC converter while operating under optimal TrgPS is theoretically high.
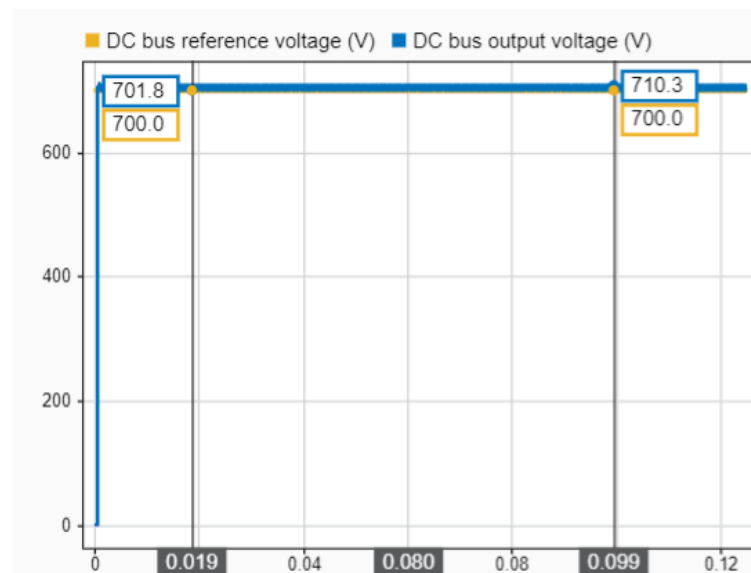

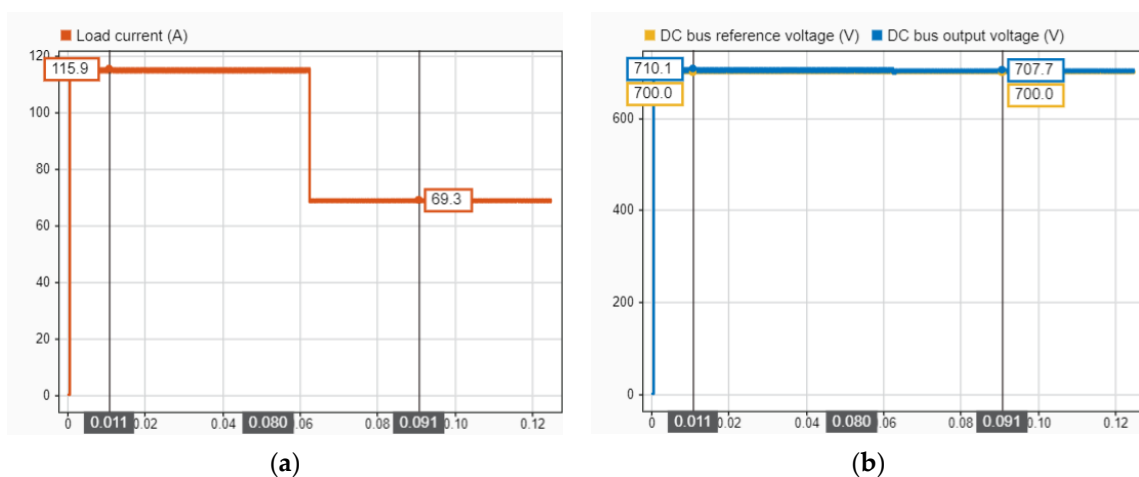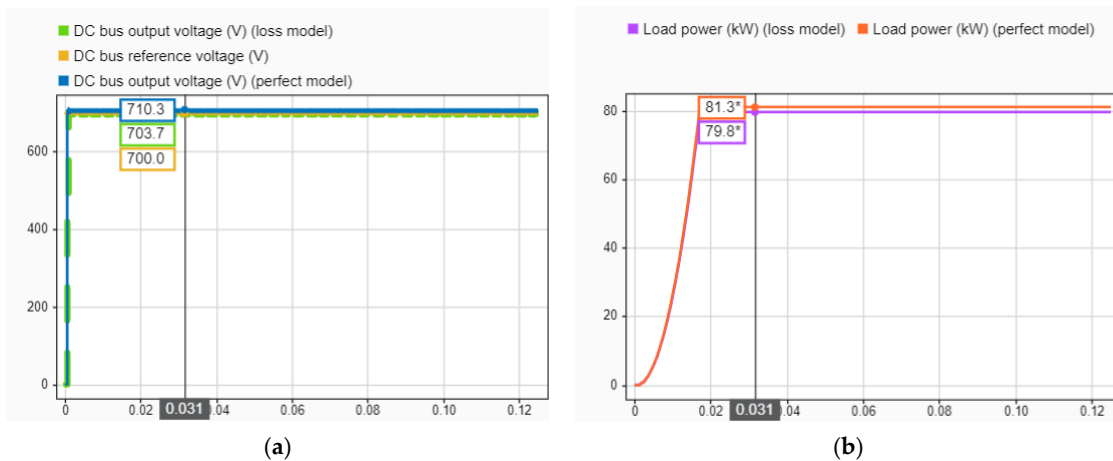**Figure 7.** Output voltage using MPC under optimal TrgPS operation.

Figure 8. Load current and output voltage for the variation of the power load from 40 kW to 10 kW: (**a**) load current; (**b**) DC bus output voltage.

Figure 9. Output voltage and load power for 40 kW using perfect model and conduction loss model for DAB DC-DC converter: (**a**) DC bus output voltage; (**b**) load power.

On the other hand, as a main feature of the DAB converter, zero-voltage switching (ZVS) is also investigated, as shown in Figures 10 and 11. It is obvious that the operation in optimal TrgPS modulation provides zero-voltage switching only for the secondary bridge alone; otherwise, the switching in the primary bridge and the turn-off switching on the secondary bridge operate under hard switching.
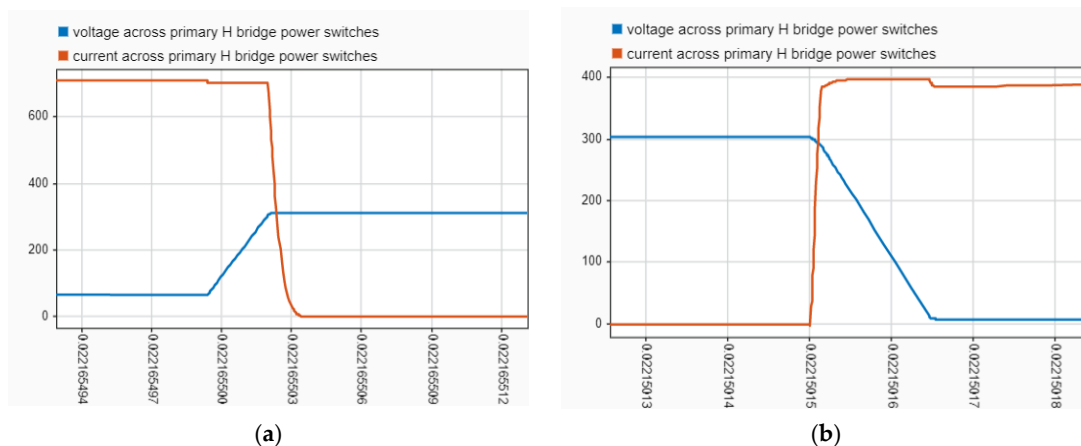

Figure 10. Current and voltage across a power switch of primary H-bridge for 80 kW DAB DC-DC converter under optimal TrgPS operation, L = 1.57 µH: (**a**) turn-off; (**b**) turn-on.
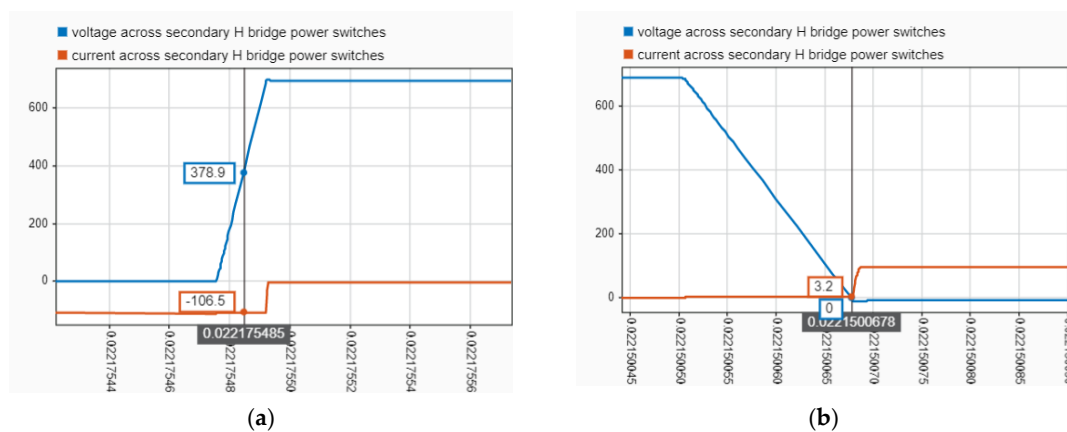
Figure 11. Current and voltage across a power switch of secondary H-bridge for 80 kW DAB DC-DC converter under optimal TrgPS operation, L = 1.57 µH: (**a**) turn-off; (**b**) turn-on.

In addition, since the input of the converter would consist of a battery, the disturbance in the input voltage should also be considered since the voltage in batteries can increase or decrease in a wide range. Figure 12 shows the output voltage response of the converter for a variation of $\pm15\%$ of the input voltage. It is obvious that under optimal TrgPS, the output voltage is not much affected by the input voltage disturbances.

(**a**)　(**b**)
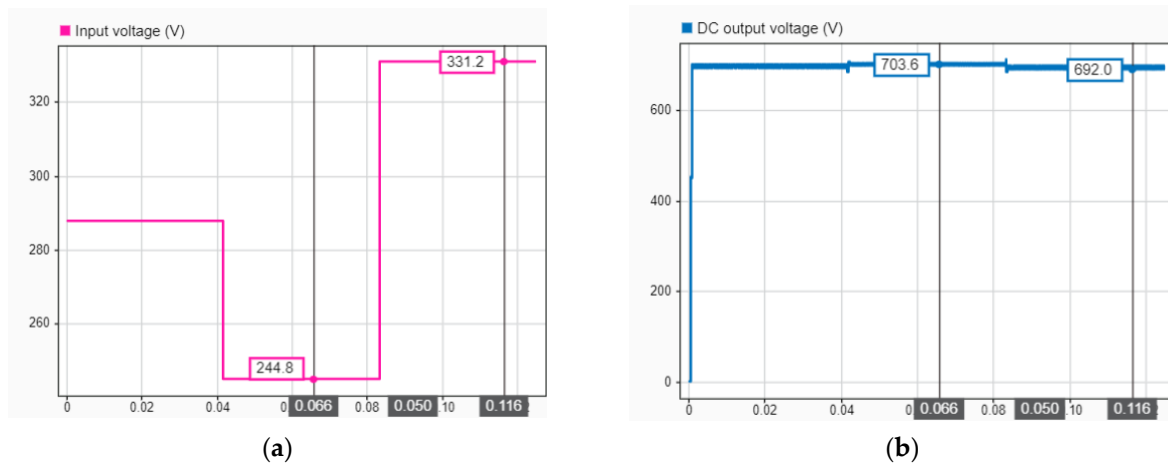
Figure 12. Input voltage disturbance response of 80 kW DAB DC-DC converter under optimal TrgPS operation, L = 1.57 μH: (**a**) input voltage disturbances; (**b**) DC bus output voltage response.

3.3.2. Optimal EPS Modulation

The upcoming analysis is realized for a DAB DC-DC converter supposed to deliver a maximum power of 80 kW ($P_n \rightarrow \frac{1}{4}$ referring to Table 1) and L = 3.15 μH, with V_1 = 288 V, V_2 = 700 V with f = 20 kHz, and C = 100 μF.

Referring to Figure 13 where the nominal power is P = 80 kW, the MPC shows also a fast response to reach the steady-state output value without any overshoot. However, the output voltage accuracy does not match the same accuracy rate as when operating in TrgPS for the same power. The output voltage error while operating in EPS is estimated to be 19%. Now, when it comes to a load variation, Figure 14 shows that the output voltage presents a better tracking of the reference voltage with a relative error estimated to be 3.2% when it comes to a lighter load (48 kW: $P_n \rightarrow \frac{d(1-d)}{2}^+$ referring to Table 1). On the other hand, Figure 15 shows that there is a slight difference when we use the perfect or conduction loss models since the maximum relative error is estimated to be almost 18% and 19%, respectively, which obviously makes the loss model a more accurate model of the converter. However, the output voltage error is still not negligible even while using a more accurate model of the converter. This voltage error is simply due to voltage drop across the power switches when operating under optimal EPS. Consequently, when it comes to the power dissipated in power switches, referring to Figure 15b, one can see that the power loss is quantified by almost 27 kW, which represents 33.7% of the power supposed to be delivered to the load (80 kW). That said, the efficiency of the DAB DC-DC converter while operating under EPS is theoretically much lower compared to operation under optimal TrgPS for the same power. Note that since the current conducted by power switches is reduced for light loads, the voltage drop effect does not affect switches' power losses at the same rate of heavy loads. However, switches' power losses are still not negligible at all. Figure 16 shows the power received by the load which is quantified by 46.9 kW for a supposed delivered power of 48 kW. The losses here are quantified by 1.1 kW, which represents 2.3% of the supposed delivered power. Compared with losses in Figure 15 (heavy load), the operation under optimal EPS for light loads provides a much lower percentage (2.3%), but it is still not negligible when quantified (1.1 kW).
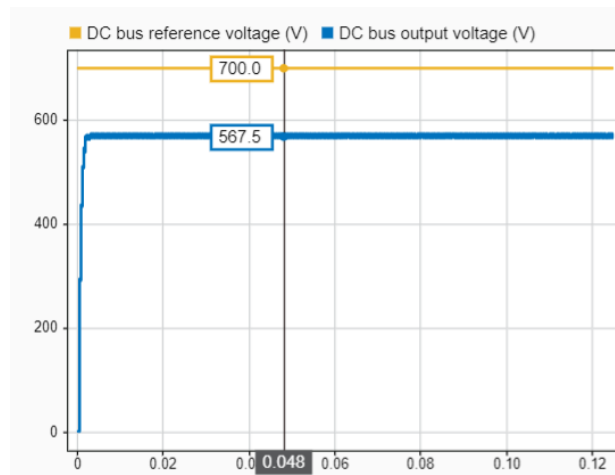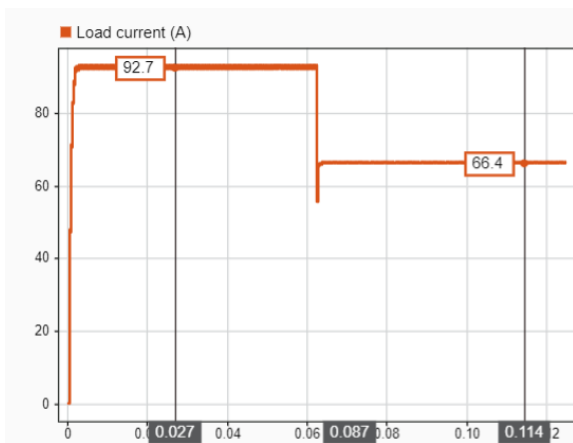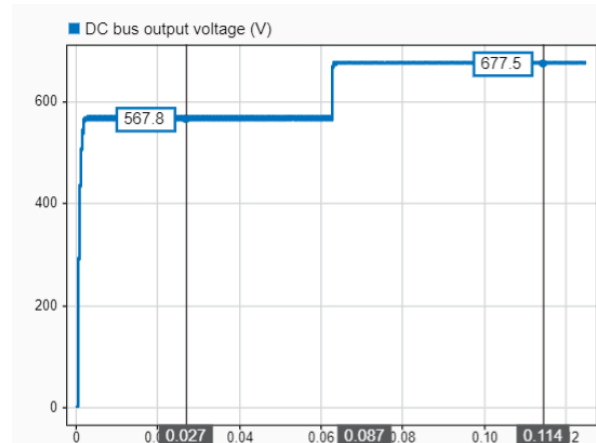
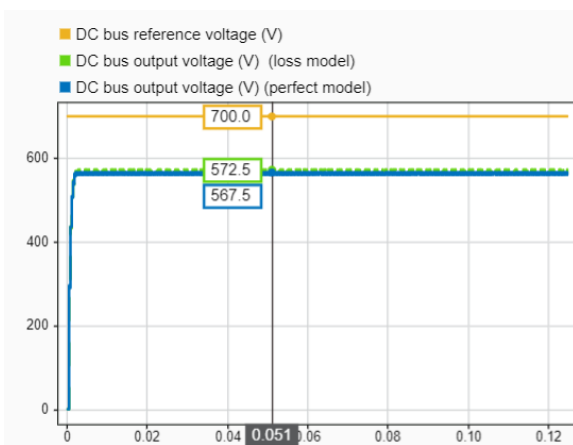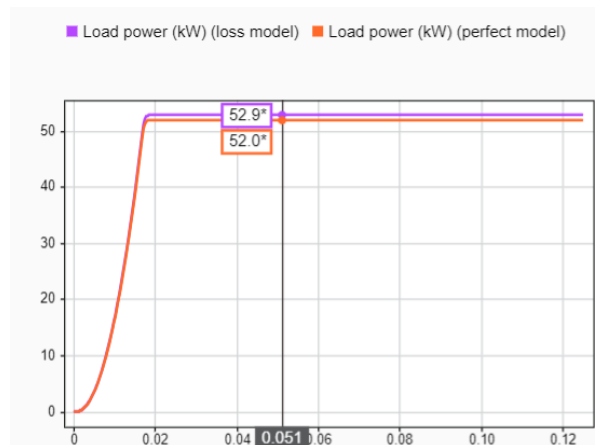**Figure 13.** Output voltage using MPC under optimal EPS operation.

(**a**)

(**b**)

Figure 14. Load current and output voltage for a variation of the power load from 80 kW to 70 kW: (**a**) load current; (**b**) DC bus output voltage.

(**a**)

(**b**)

Figure 15. Output voltage and load power for 80 kW using perfect model and conduction loss model for DAB DC-DC converter: (**a**) DC bus output voltage; (**b**) load power.
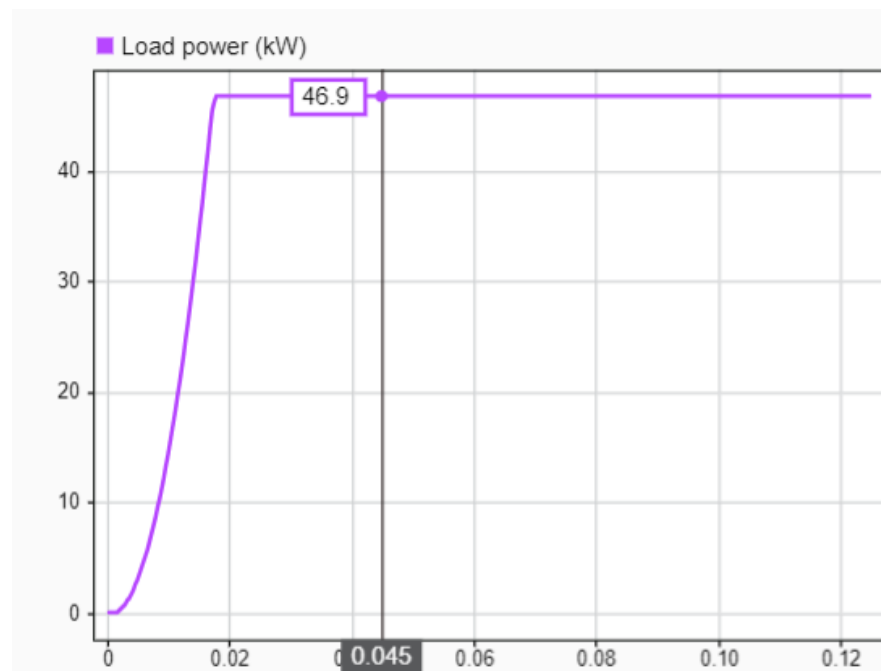
Figure 16. Load power for a supposed delivered power of 48 kW under optimal EPS operation.

On the other hand, zero-voltage switching (ZVS) is also investigated, as shown in Figures 17 and 18. It is obvious that operation under optimal EPS offers zero-voltage switching for both primary and secondary bridges. However, the turn-off of the power switches for both bridges is a hard turn-off. Soft switching is an important feature provided by the DAB converter. This feature will allow a minimization of switching losses which will lead to less heat dissipation in the power switches and thus optimize the design of the converter's heat sink. However, even by providing this advantageous feature, the operation under optimal EPS is suffering from important power switches' losses. Precisely, it suffers from power switches' conduction losses since the switching losses are minimized, as depicted by Figures 15b, 17 and 18.
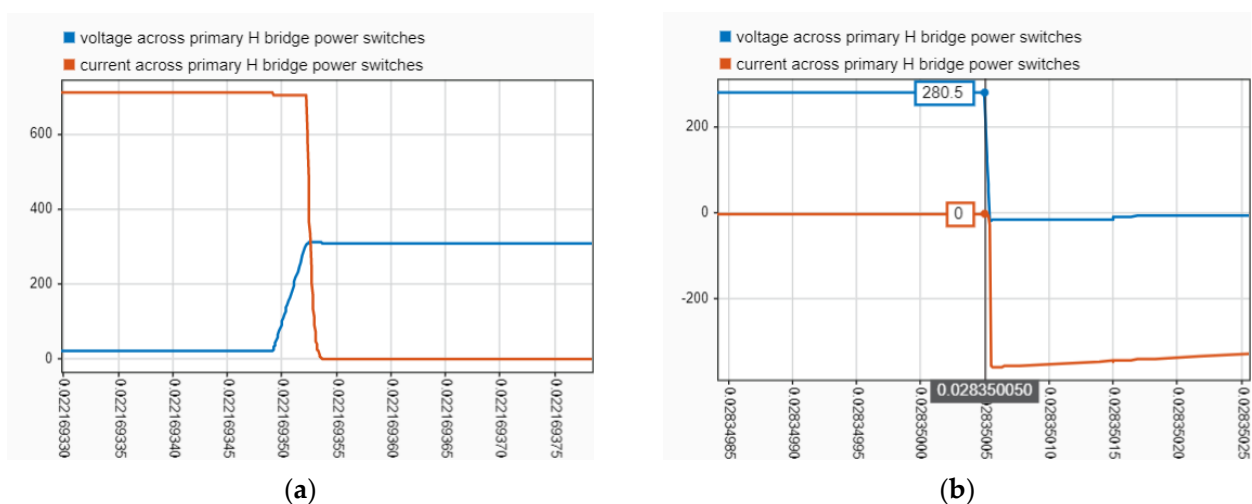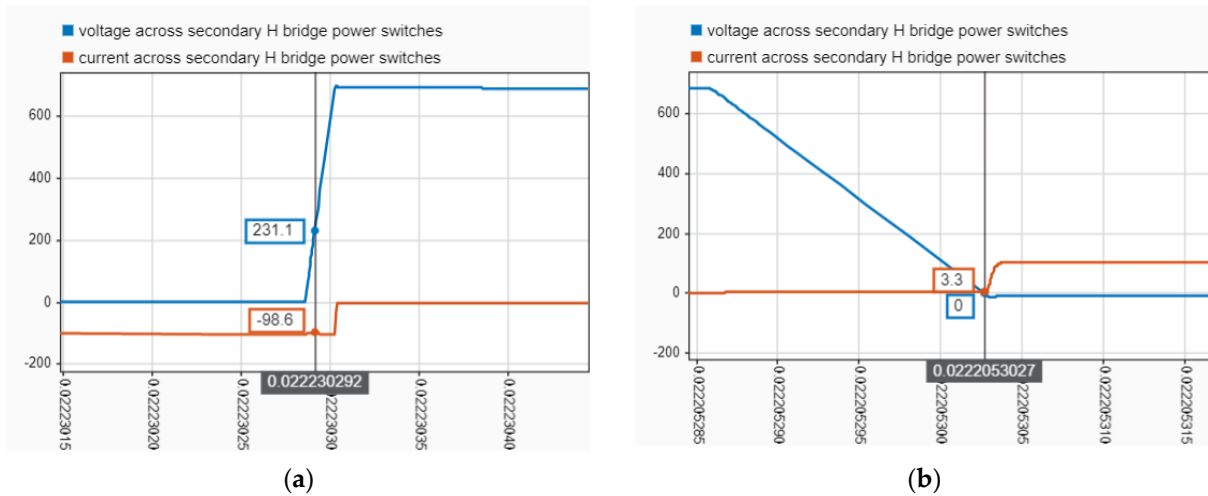

Figure 17. Current and voltage across a power switch of primary H-bridge for 80 kW DAB DC-DC converter under optimal EPS operation, L = 3.15 μH: (**a**) turn-off; (**b**) turn-on.

(**a**)　(**b**)

Figure 18. Current and voltage across a power switch of secondary H-bridge for 80 kW DAB DC-DC converter under optimal EPS operation, L = 3.15 μH: (**a**) turn-off; (**b**) turn-on.

The input voltage disturbance is also considered while operating under optimal ESP in the same conditions, i.e., a variation of ±15% of the input voltage, as shown in Figure 19. One can see that the output voltage is not stable and the error increases drastically when the input voltage decreases.

(**a**)　(**b**)
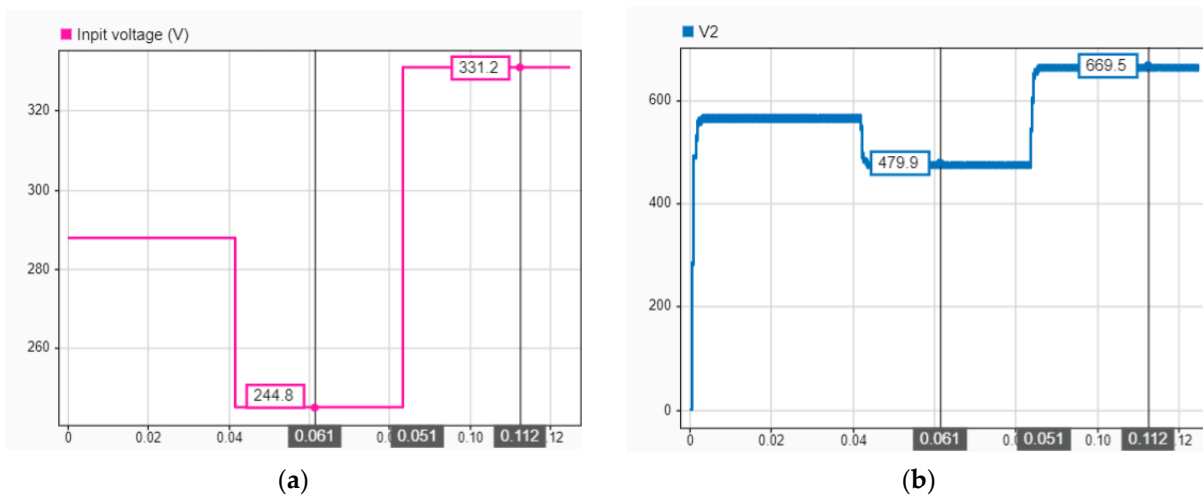
Figure 19. Input voltage disturbance response of 80 kW DAB DC-DC converter under optimal EPS operation, L = 3.15 μH: (**a**) input voltage disturbances; (**b**) DC bus output voltage response.

4. Performance Comparison of Operation under Optimal TrgPS and Optimal EPS Modulation Techniques

Referring to the analysis presented in previous sections, Table 3 summarizes the performance of both optimal TrgPS (L = 1.57 μH) and optimal EPS (L = 3.15 μH) based on different constraints for the same rated power (80 kW). It is obvious that the operation of the DAB converter under optimal TrgPS modulation offers a better tracking of the desired output voltage, is more efficient, and does not get affected by input voltage disturbances compared with operation under optimal EPS. The only advantage that optimal EPS provides is ZVS-on for both primary and secondary H-Bridges. This is not the case while operating under optimal TrgPS, which provides ZVS-on only for the secondary H-Bridge. In fact, the lack of efficiency during operation under optimal EPS is caused by the phase angle between the primary bridge voltage and the inductor current, as explained in a more general way in Figure 3. This leads to the increase in the circulating current which produces more power switches' conduction losses. On the other hand, the operation under optimal

triangular PS modulation provides a minimal phase angle between the primary bridge voltage and inductor current. In that case, the circulating current is minimized and so are the conduction losses of power switches. Figure 20 shows the primary bridge voltage, the secondary voltage brought to the primary, and the inductor current for the operation in both optimal TrgPS modulation and EPS modulation for the same power of 80 kW. One can see that in fact the inductor current is actually in phase with the primary voltage in Figure 20a, which is not the case when operating under EPS mode, shown in Figure 20b.

Table 3. Circuit parameters' variation with respect to EPS operating mode.

| Constraints	Optimal TrgPS	Optimal EPS
Reference voltage tracking	Negligible error for both heavy and light loads	Important error for both heavy and light loads (the error increases drastically for heavy loads)
Power losses	Negligible	Acceptable for light loads (but still important when quantified), not acceptable for heavy load
Soft switching	ZVS-on only for secondary H-Bridge	ZVS-on for both primary and secondary H-Bridge
Input voltage disturbance effect	Does not affect the operation	Affects the operation drastically

(**a**)

(**b**)
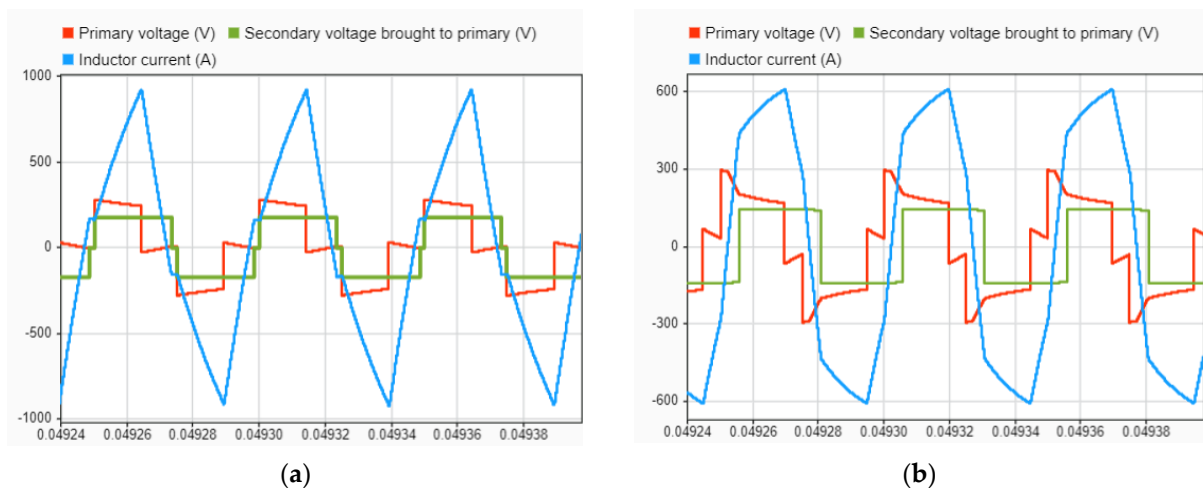
Figure 20. Primary voltage, secondary voltage brought to the primary, and inductor currents for 80 kW DAB DC-DC converter: (**a**) operation under optimal TrgPS; (**b**) operation under optimal EPS.

Another feature provided by the operation under optimal TrgPS modulation in the same case study is the reduced size of magnetic components. In fact, in order to operate the DAB DC-DC converter for the same power (80 kW), the inductance value changes from operation under optimal TrgPS modulation to operation under optimal EPS according to Equations (3) and (4). Therefore, this change in inductance value affects the inductor's and the transformer core's designs. To design an inductor and a transformer, two main equations are required to determine the area product of the magnetic cores of both components. These equations are shown respectively in (28) and (29).

$$\frac{L I_m I_{rms}}{K_w B_m J} = A_c A_w = A \tag{28}$$

$$\frac{V_{ab} I_{rms}}{2 K_w B_m J f} = A_c A_w = A \tag{29}$$

with:

I_m: peak current of the inductor/transformer
I_{rms}: peak rms current of the inductor/transformer
K_w: window space factor
B_m: maximum flux density of the core material
J: maximum current density of the conductor
A_c: the cross-section area which represents the area of the magnetic path
A_w: the window area which represents the area of conductor path
A: area product of the magnetic core

Figure 21 shows both the peak current and root mean square (rms) current of the inductor while operating under 80 kW for both optimal EPS (L = 3.15 µH) and optimal TrgPS (L = 1.57 µH).

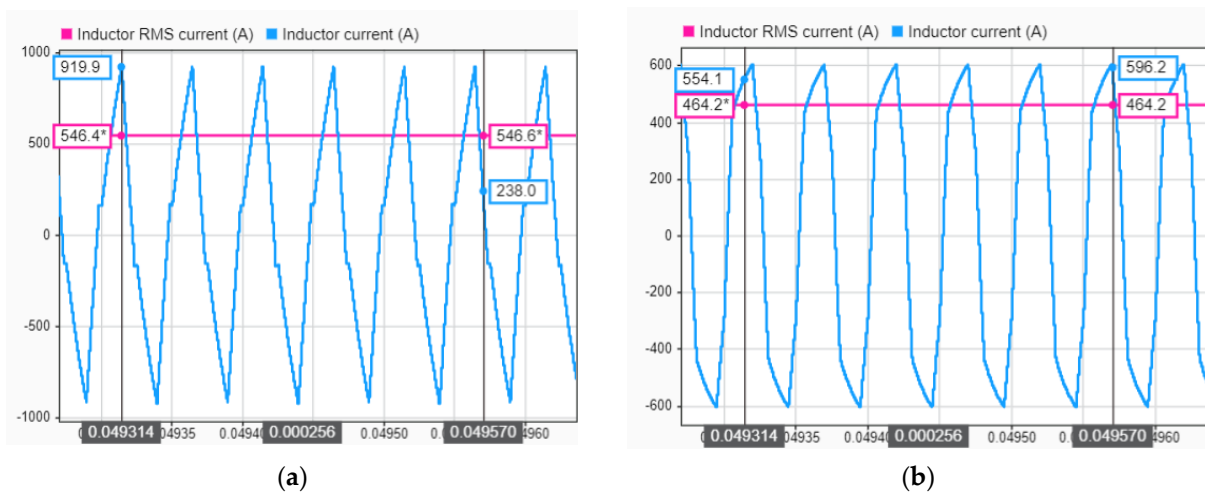(**a**)   (**b**)

Figure 21. Peak and RMS currents for 80 kW DAB DC-DC converter: (**a**) operation under optimal TrgPS; (**b**) operation under optimal EPS.

Taking the circuit parameters of operation under optimal EPS as a reference, for an inductance value reduced by 50% (L = 3.15 µH to L = 1.57 µH), the peak current increases by 54% and the rms current decreases by 3.2%. When it comes to operation under TrgPS modulation, according to Equations (28) and (29), this leads to a decrease in the product area of approximatively 36% and a reduction in the product area of the transformer core of approximately 9%, as summarized in Table 4.

**Table 4.** Circuit parameter variation with respect to optimal EPS operating mode.

Circuit Parameters	EPS Operation	TrgPS Operation	Variation with Respect to EPS (Per Unit)
Inductance (µH)	3.15	1.57	−0.502
Peak current (A)	596	920	+0.54
RMS current (A)	564	546	−0.032
Primary RMS voltage (V)	270	254	−0.06
Inductor's core product area (per unit)	1	0.74	−0.36
Transformer's core product area (per unit)	1	0.91	−0.09

In other words, to operate the DAB DC-DC converter for a nominal power of 80 kW, the operation under optimal TrgPS modulation improves the converter's efficiency and its output voltage accuracy and minimizes the sizes of the inductor and transformer cores. Note that the inductor and transformer masses and volumes represent an important percentage of the total mass and volume of the converter.

The efficiency of the DAB DC-DC converter along with the feature of reducing the magnetic components' weights and sizes are further investigated for different values of nominal power for operation under both optimal TrgPS and optimal EPS, as shown in Figures 22–24.
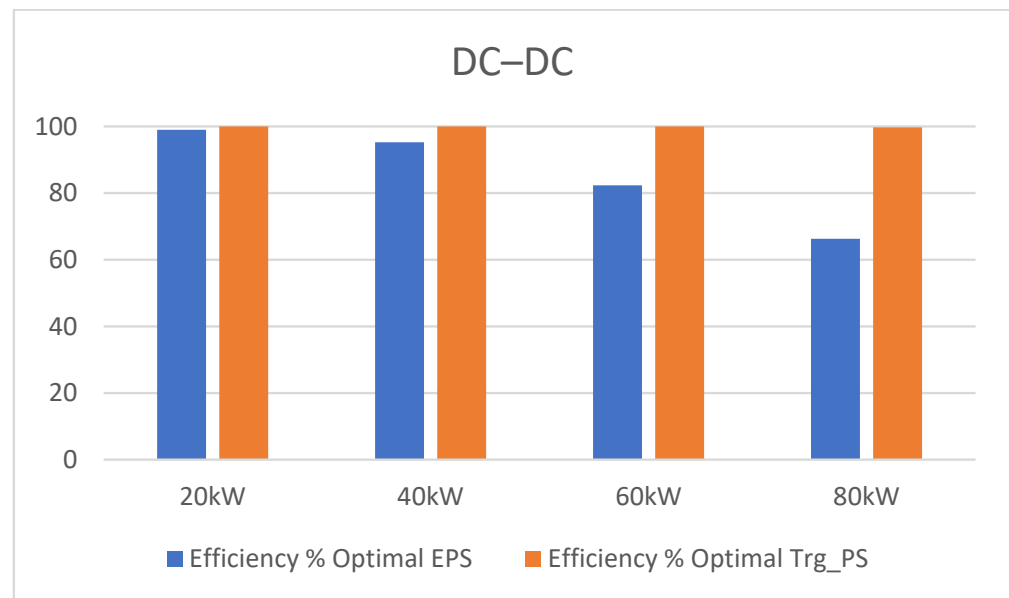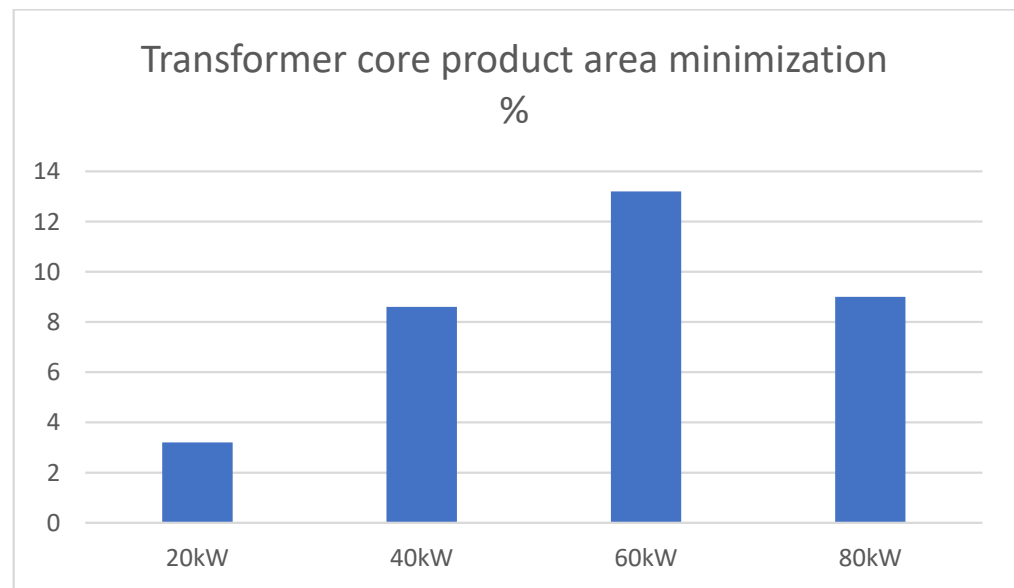

Figure 22. Efficiency of DAB DC-DC converter for different values of nominal power for operation under both optimal TrgPS and optimal EPS.
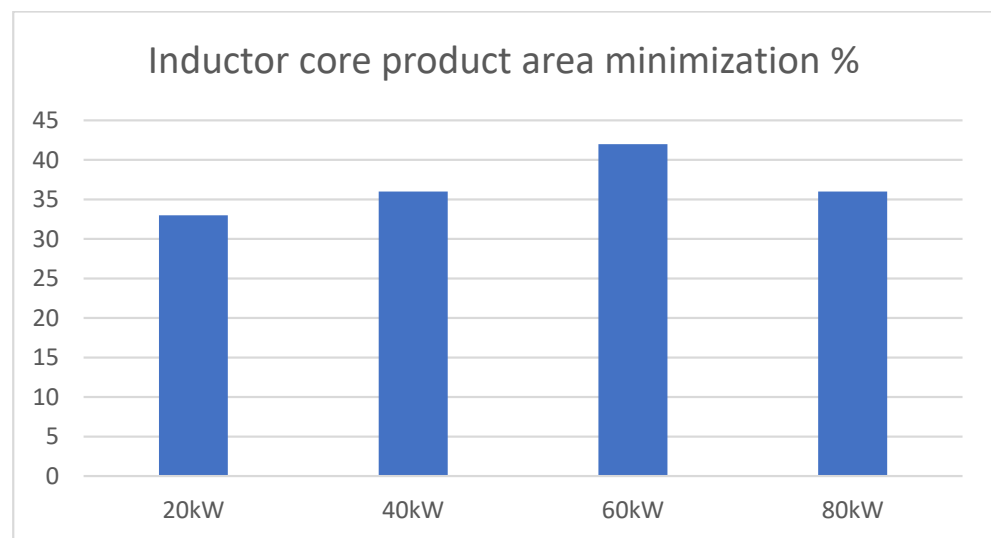
Figure 23. Inductor core product area minimization rate for operation under optimal TrgPS with respect to optimal EPS operation for different values of nominal power.

It is obvious that the efficiency of the DAB DC-DC converter under optimal TrgPS operation is greater than the efficiency of operation under optimal EPS modulation when it comes to nominal power of the converter greater than 20 kW. In addition, the inductor and transformer product core areas for operation under optimal TrgPS are also reduced in comparison with operation under optimal EPS for the same nominal power values.

Combining the results of Table 4 and Figures 22–24, it is obvious that for a DAB DC-DC converter at high power, operation under optimal TrgPS modulation is the most suitable and optimal modulation technique when it comes to reactive power minimization in power switches and magnetic components' weight and size reduction.

Figure 24. Transformer core product area minimization rate for operation under optimal TrgPS with respect to optimal EPS operation for different values of nominal power.

5. Discussion

The aim of the analysis realized above consists of the selection of a suitable modulation technique for the DAB DC-DC converters of BEVs' powertrains. MPC is arbitrarily chosen as a control approach due to its superiority and advantageous features provided in comparison with conventional PID control. Two modulation techniques are compared, optimal TrgPS and optimal EPS, for the same nominal power of DAB DC-DC converter. Compared to optimal EPS modulation, operation under optimal TrgPS provides the following features: it has a better tracking of the reference voltage, a much better efficiency, it does not get much affected by input voltage disturbances, and it has the abilities to provide ZVS-on (even if it is only for the secondary H-Bridge), and to reduce the weights and sizes of magnetic components (inductor and transformer). Another feature provided by operation under TrgPS modulation is the elimination of the transient load problem. In fact, referring to the analysis presented in Section 2, more precisely, Table 1, during operation under optimal TrgPS at nominal power, the converter power is always limited to an upper limit $P_n \to \frac{d(1-d)}{2}^-$. However, during operation under optimal EPS modulation, the converter power has one lower limit which is also its upper limit in some cases ($P_n \to \frac{d(1-d)}{2}^-$ or $P_n \to \frac{d(1-d)}{2}^+$) depending on the amount of power load requested. Here, we talk about transient loads, i.e., when the power demand will fluctuate between the two modes of operation. Note that such an operation would require a more refined global control which will increase the computational capacity of the controller when it comes to fluctuating loads' demands, and thus, the global control would be more complex, thus more expensive.

Optimal EPS modulation can be used for low power where the efficiency does not get affected by power switches' reactive power, as shown in Figure 22. However, the transient load problem would always exist and would need meticulous study depending on the specific case study. Since optimal EPS provides high efficiency only for relatively low nominal power application compared to the power demand of BEVs' powertrains, this modulation technique would not be of interest at all. That said, all these features mentioned above make operation under the optimal TrgPS modulation technique at nominal power a more suitable and optimal modulation technique for DAB DC-DC converters meant for BEV powertrain application.

6. Conclusions

It is true that the analysis presented in this paper shows the superiority of optimal TrgPS modulation over optimal EPS modulation when it comes to DAB DC-DC converters meant for BEV powertrain application. However, many different points that are not mentioned in this current study should be addressed in future works. These points first consist of choice and selection criteria of MPC or a different control approach, i.e., is MPC the most suitable control approach of DAB DC-DC converters meant for BEV powertrain application? The use of wideband gap power switches should also be investigated, in addition to the selection of the transformer turns ratio selection and how these variables would affect the performance of DAB DC-DC converter operation. Only one thing was cleared out in this paper: optimal TrgPS modulation is the most suitable and optimal modulation technique for DAB DC-DC converters meant for BEV powertrain application.

Conflicts of Interest: The authors declare no conflict of interest.

References

1. Mersky, A.C.; Sprei, F.; Samaras, C.; Qian, Z. (Sean) Effectiveness of Incentives on Electric Vehicle Adoption in Norway. *Trans. Res. Part D Trans. Environ.* **2016**, *46*, 56–68. [CrossRef]
2. Matthews, L.; Lynes, J.; Riemer, M.; Del Matto, T.; Cloet, N. Do We Have a Car for You? Encouraging the Uptake of Electric Vehicles at Point of Sale. *Energy Policy* **2017**, *100*, 79–88. [CrossRef]
3. Das, H.S.; Tan, C.W.; Yatim, A.H.M. Fuel Cell Hybrid Electric Vehicles: A Review on Power Conditioning Units and Topologies. *Renew. Sustain. Energy Rev.* **2017**, *76*, 268–291. [CrossRef]
4. Lin, B.; Wu, W. Why People Want to Buy Electric Vehicle: An Empirical Study in First-Tier Cities of China. *Energy Policy* **2018**, *112*, 233–241. [CrossRef]
5. Sarlioglu, B.; Morris, C.T.; Han, D.; Li, S. A Review of Technological Improvements for Electric Machines, Power Electronics, and Batteries for Electric and Hybrid Vehicles. *IEEE Ind. Appl. Mag.* **2017**, *23*, 14–25. [CrossRef]
6. Piques, J.-D. SysML for Embedded Automotive Systems: SysCARS Methodology. In Proceedings of the Embedded Real Time Software and Systems (ERTS2014), Toulouse, France, 5–7 February 2014.
7. Doufene, A.; Dauron, A.; Krob, D. 2.1.1 Model-Based Operational Analysis for Complex Systems—A Case Study for Electric Vehicles. *INCOSE Int. Symp.* **2014**, *24*, 122–138. [CrossRef]
8. Hicham, E.H.; Ahmed, C.; Mourad, Z. Model-Based System Engineering Design of a Versatile Control Test Bench of an Electric Vehicle's Powertrain for Educational Purpose. In Proceedings of the 2021 3rd Global Power, Energy and Communication Conference (GPECOM), Antalya, Turkey, 5–8 October 2021; pp. 233–239.
9. Hadraoui, H.E.; Chebak, A.; Zegrari, M. Design of a Versatile Diagnostic Test Bench of an Electric Vehicle's Powertrain for Educational Purpose Using a Model-Based System Engineering. *E3S Web Conf.* **2022**, *336*, 00058. [CrossRef]
10. Guennouni, N.; Machkour, N.; Chebak, A. Using MBSE for Operational Analysis of Power Converter for Electric Traction. In Proceedings of the 2021 17th Conference on Electrical Machines, Drives and Power Systems (ELMA), Sofia, Bulgaria, 1–4 July 2021; pp. 1–6.
11. Jain, A.K.; Ayyanar, R. Pwm Control of Dual Active Bridge: Comprehensive Analysis and Experimental Verification. *IEEE Trans. Power Electron.* **2011**, *26*, 1215–1227. [CrossRef]
12. Xie, Y.; Sun, J.; Freudenberg, J.S. Power Flow Characterization of a Bidirectional Galvanically Isolated High-Power DC/DC Converter Over a Wide Operating Range. *IEEE Trans. Power Electron.* **2010**, *25*, 54–66. [CrossRef]
13. Huang, J.; Wang, Y.; Li, Z.; Lei, W. Unified Triple-Phase-Shift Control to Minimize Current Stress and Achieve Full Soft-Switching of Isolated Bidirectional DC–DC Converter. *IEEE Trans. Ind. Electron.* **2016**, *63*, 4169–4179. [CrossRef]
14. Hou, N.; Song, W.; Wu, M. mingyi Minimum-Current-Stress Scheme of Dual Active Bridge DC-DC Converter with Unified-Phase-Shift Control. *IEEE Trans. Power Electron.* **2016**, *31*, 8552–8561. [CrossRef]
15. Tong, A.; Hang, L.; Li, G.; Jiang, X.; Gao, S. Modeling and Analysis of a Dual-Active-Bridge-Isolated Bidirectional DC/DC Converter to Minimize RMS Current With Whole Operating Range. *IEEE Trans. Power Electron.* **2018**, *33*, 5302–5316. [CrossRef]
16. Zhao, B.; Yu, Q.; Sun, W. Extended-Phase-Shift Control of Isolated Bidirectional DC–DC Converter for Power Distribution in Microgrid. *IEEE Trans. Power Electron.* **2012**, *27*, 4667–4680. [CrossRef]

17. Zhao, B.; Song, Q.; Liu, W. Efficiency Characterization and Optimization of Isolated Bidirectional DC–DC Converter Based on Dual-Phase-Shift Control for DC Distribution Application. *IEEE Trans. Power Electron.* **2013**, *28*, 1711–1727. [CrossRef]
18. Zhao, B.; Song, Q.; Liu, W. Power Characterization of Isolated Bidirectional Dual-Active-Bridge DC–DC Converter With Dual-Phase-Shift Control. *IEEE Trans. Power Electron.* **2012**, *27*, 4172–4176. [CrossRef]
19. Zhao, B.; Song, Q.; Liu, W.; Sun, W. Current-Stress-Optimized Switching Strategy of Isolated Bidirectional DC–DC Converter With Dual-Phase-Shift Control. *IEEE Trans. Ind. Electron.* **2013**, *60*, 4458–4467. [CrossRef]
20. Choi, W.; Rho, K.-M.; Cho, B.-H. Fundamental Duty Modulation of Dual-Active-Bridge Converter for Wide-Range Operation. *IEEE Trans. Power Electron.* **2016**, *31*, 4048–4064. [CrossRef]
21. Shi, H.; Wen, H.; Chen, J.; Hu, Y.; Jiang, L.; Chen, G. Minimum-Reactive-Power Scheme of Dual-Active-Bridge DC–DC Converter With Three-Level Modulated Phase-Shift Control. *IEEE Trans. Ind. Appl.* **2017**, *53*, 5573–5586. [CrossRef]
22. Shao, S.; Jiang, M.; Ye, W.; Li, Y.; Zhang, J.; Sheng, K. Optimal Phase-Shift Control to Minimize Reactive Power for a Dual Active Bridge DC–DC Converter. *IEEE Trans. Power Electron.* **2019**, *34*, 10193–10205. [CrossRef]
23. Zhao, B.; Song, Q.; Liu, W.; Liu, G.; Zhao, Y. Universal High-Frequency-Link Characterization and Practical Fundamental-Optimal Strategy for Dual-Active-Bridge DC-DC Converter Under PWM Plus Phase-Shift Control. *IEEE Trans. Power Electron.* **2015**, *30*, 6488–6494. [CrossRef]
24. Syed, I.; Xiao, W.; Zhang, P. Modeling and Affine Parameterization for Dual Active Bridge DC-DC Converters. *Electric Power Compon. Syst.* **2015**, *43*, 665–673. [CrossRef]
25. Li, K.; Yang, Y.; Tan, S.-C.; Hui, R.S.-Y. Sliding-Mode-Based Direct Power Control of Dual-Active-Bridge DC-DC Converters. In Proceedings of the 2019 IEEE Applied Power Electronics Conference and Exposition (APEC), Anaheim, CA, USA, 17–21 March 2019; pp. 188–192.
26. Tiwary, N.; Venkataramana, N.N.; Panda, A.K.; Narendra, A. Direct Power Control of Dual Active Bridge Bidirectional DC-DC Converter. In Proceedings of the 2019 International Conference on Power Electronics, Control and Automation (ICPECA), New Delhi, India, 16–17 November 2019; pp. 1–4.
27. Borreggine, S.; Monopoli, V.G.; Rizzello, G.; Naso, D.; Cupertino, F.; Consoletti, R. A Review on Model Predictive Control and Its Applications in Power Electronics. In Proceedings of the 2019 AEIT International Conference of Electrical and Electronic Technologies for Automotive (AEIT AUTOMOTIVE), Turin, Italy, 2–4 July 2019; pp. 1–6.
28. Karamanakos, P.; Liegmann, E.; Geyer, T.; Kennel, R. Model Predictive Control of Power Electronic Systems: Methods, Results, and Challenges. *IEEE Open J. Ind. Appl.* **2020**, *1*, 95–114. [CrossRef]